Safety Checkpoints

Published paper @DOI: 10.1109/MMM.2016.2538514

Safety Checkpoints

Kazemipour A., Kleine-Ostmann T., Schrader T., Allal D., Charles M., Zilberti L., Borsero M., Bottauscio O., Chiampi M.

With the advent of new applications such as more sophisticated airport security scanners, people will increasingly be exposed to millimeter- and submillimeter-wave radiation. While the question of whether non-ionizing electromagnetic radiation has any nonthermal biological effects remains subject to debate, the thermal effects of electromagnetic radiation are clearly evident. Based on studies performed predominantly at lower frequencies, safety limits have been set by the International Commission for Non-Ionizing Radiation Protection [1]. Between 2 and 300 GHz, the safety limit in terms of power flux density is 1 mW/cm^2. This safety limit is derived from the basic limits defined for a specific absorption rate (SAR) between 100 kHz and 10 GHz of 0.08 W/kg for a body overall and of 2 W/kg for a limb. These SAR values exhibit a safety factor of 50 with regard to previously proven thermal health effects.

Measurement studies have been performed to determine the strength, in general terms, of the radiated electromagnetic fields in security scanners. However, due to variations among the emitted fields in time, frequency, and space, measuring these power densities accurately is a nontrivial matter [2]. The approach we have taken is based on measuring the power density using a calibrated spectrum analyzer with an external mixer and a calibrated horn antenna. From the measured (and corrected) power level P and the antenna gain g, the power density at the antenna location can be determined by

$$S = \frac{P}{A_{\text{eff}}} = \frac{P}{g \cdot \frac{c^2}{4\pi f^2}} = \frac{4\pi f^2}{g \cdot c^2} P,$$

where A_{eff} is the effective antenna area, f is the frequency, and c the speed of light [3]. Using calibrated measurement equipment allows traceability to the International System of Units (SI). Measurement studies have shown that the maximum emission of security scanners is many orders of magnitude below the safety limits [4].

To find out how a radiated power density—either a plane wave in the far field or a collimated Gaussian beam—relates to heat induced in the human body, we have taken a numerical modeling approach implemented as a "homemade" finite element method (FEM) tool. Because the penetration depth of millimeter-wave and terahertz radiation is well below 1 mm, it is mainly the skin that is affected, but adjacent tissues also have to be modeled to provide the correct boundary conditions, especially for the thermal problem. In a second step, we verified results based on thermal infrared imaging of a skin phantom during illumination with millimeter waves.

Electromagnetic and Thermal Models

The heating induced by millimeter and submillimeter electromagnetic radiation inside the human body cannot be measured directly, but it can be estimated either by numerical computations in human models or by

experiments performed on phantoms. Even though the phantoms suitable for this application are now quite primitive, they can still provide a useful tool for validating the accuracy of the computational techniques.

The computational approach requires a model of human tissues that includes both the electrical (i.e., electrical conductivity and permittivity) and thermal (i.e., thermal conductivity, per-unit volume heat capacity, and blood perfusion coefficient) properties of each tissue, as well as a numerical tool able to solve the electromagnetic and thermal field problems.

For the frequency band of interest, the low penetration of the electromagnetic waves implies that only the most external tissues are involved in the phenomena. This feature allows the use of simplified models (e.g., stratified disposition) with a limited number of tissues and does not require complex representations of the human body with numerous materials (e.g., voxel models). The electrical and thermal parameters are available on some online databases [5], [6], but these are not free from uncertainty or possible value spread because of the natural variability in the structure and composition of biological tissues.

In particular, when data presented by different authors [7]–[9] are compared, a very large variability is found in the electrical properties of biological tissues at 1 THz. This large range of variation in tissue properties has stimulated the development of parametric analyses [10] and the adoption of statistical tools [11] to investigate the influence of tissue parameters in the thermal response of bodies exposed to millimeter and submillimeter electromagnetic waves.

Based on the assumption that tissue properties are not modified by a limited temperature elevation (as a posteriori verified), the numerical approach can be divided into the solving of two successive and separate field problems:

1) the electromagnetic solution, i.e., predicting the propagation of the electromagnetic field inside the tissues and the power density deposited by the wave
2) the thermal problem, i.e., estimating the temperature elevation resulting from the power deposition and its diffusion in space and time.

A complete solution of the field propagation problem would be computationally demanding because of the three-dimensional (3-D) characteristics of the wave, the open-boundary domain, and the fine level of discretization imposed by the wavelength at the frequency of interest. The computational burden is significantly reduced if we consider a flat, stratified model of the human tissues (indefinite on the *xy*-plane, with the final layer extending to infinite) exposed to a continuous, uniform, and linearly polarized plane wave, normally incident to the surface of the model [see Figure 1(a)].

Under these reasonable assumptions, the wave propagation becomes a one-dimensional problem governed by the Helmholtz equation. The analytical solution for the electric (**E**) and magnetic (**H**) fields in each layer is the superposition of a progressive and a regressive wave (the coefficients of which are determined by imposing the continuity of **E** and **H** across all the interfaces), by assuming the amplitude of the incident wave on the body surface as the driving term and by adopting a zero value for the regressive wave in the deepest layer. This solution also provides an analytical expression of the distribution of the dissipated average volume power density, which is the source for the thermal problem.

The evolution of the temperature inside the body model is described by the Pennes bioheat equation, which, in its most general case, includes five terms: thermal conduction, blood-perfusion effect, metabolic heating, electromagnetic heating, and heat storage. By expressing the same equation in terms of temperature elevation with respect to a steady-state temperature distribution before exposure, the contributions of the metabolic heating and of the blood temperature become implicit.

The problem can then be set by imposing the Robin convection condition at the interface with air, the continuity of temperature and thermal flux across the internal interfaces between the layers, and a null temperature elevation at infinite. The equation can be further simplified when predicting the steady-state temperature produced by a continuous radiation: in such a problem, the term of the heat storage vanishes, and an analytical solution is available.

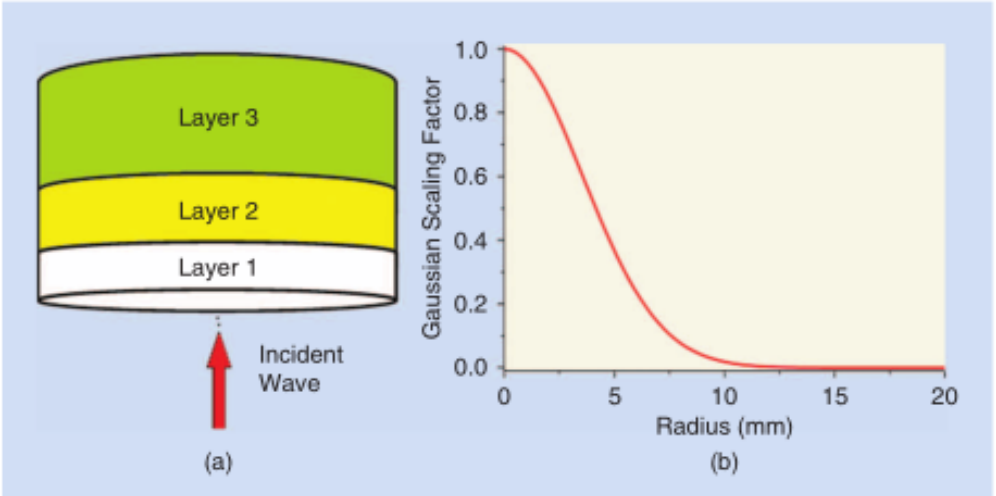

Figure 1. *The electromagnetic model: (a) the scheme of the stratified human model adopted for solving the electromagnetic wave propagation problem and (b) the Gaussian scaling factor imposed on the volume power density deposited by the electromagnetic wave.*

Unfortunately, this analytical solution for the coupled electromagnetic and thermal problems is too conservative and not very realistic. The radiation is not uniformly distributed over the whole body surface; rather, it is localized by the beam to a restricted zone. Moreover, the radiation is not applied continuously but only for a limited time interval.

A more realistic representation of the wave source is given by a Gaussian focused beam. This makes the thermal problem (in terms of temperature elevation) a 3-D axial-symmetric problem, defined in a cylindrical domain sufficiently large to allow the imposition of a null temperature elevation on all external surfaces, apart from the frontal interface with air. The solution is obtained through the FEM method where first-order elements are used and the unknowns are the nodal values of the temperature elevation. Under dynamic operating conditions, the FEM solution is inserted into a step-by-step computational scheme and can account for the presence of the heat storage term in the Pennes equation. Finally, to simulate the effects of the focused beam, the spatial distribution of the thermal power density is properly weighted within the tissues according to a Gaussian profile [12].

TABLE 1. The electrical and thermal properties of different tissues.

		Skin	SAT	Muscle
Relative permittivity ε_r	25 GHz	18.3	6.4	26.6
	100 GHz	6.4	3.67	8.63
	1 THz	2.8	2.44	3.12
Electrical conductivity σ (S/m)	25 GHz	23.6	4.58	30.5
	100 GHz	34.0	10.6	62.5
	1 THz	44.8	41.9	59.4
Thickness (mm)		1.15	3.5	–
Thermal conductivity λ [W/(m K)]		0.37	0.21	0.49
Perfusion coefficient h_b [W/(m^3 K)]		7441	1903	2691
Heat capacity per unit volume c_v [MJ/(m^3 K)]		3.76	2.14	3.73

Simulation Results

Human tissues are represented through a stratified structure composed of three homogeneous layers: the skin, subcutaneous adipose tissue (SAT), and muscle. The muscle depth is assumed to be sufficiently large (40 mm) that its artificial boundary does not alter the results. The values of the skin and SAT layer thicknesses are presented in Table 1, together with the thermal and electrical properties of all tissues for 0.025, 0.1, and 1 THz.

In all the simulations, the power density developed by an incident, linearly-polarized plane wave is preliminarily computed analytically. The wave carries, under unperturbed conditions, a 1-W/m^2 power density on the body surface, but the results (distributions of the temperature elevation) can be scaled linearly with this quantity. When solving the thermal problem, the computational domain is reduced to a stratified cylinder (radius = 80 mm) as illustrated in Figure 1(a), where the 1-W/m^2 power density is focused around the central axis according to the Gaussian profile presented in Figure 1(b). The radiation is switched off after 1 s, but the heating diffusion is analyzed during a time interval of 8 s.

Figure 2 presents the distributions of per-unit volume power density deposited in the tissues along the depth of the domain for all the considered frequencies. The penetration is deeper for the lower frequencies, but, in any case, the power density practically vanishes outside the skin layer. A variation in the curve slope always arises at the interface between the skin and SAT, but it is noticeable only for the lowest frequency.

The spatial distributions of the temperature elevation and their evolution over time are summarized in the thermal maps shown in Figure 3 (at the end of the exposure time t = 1 s) and Figure 4 (at t = 8 s). These results reveal that the highest frequency gives rise to the highest value of temperature elevation. Its effect, however, is significant only for a depth less than 1 mm, whereas, at 0.025 THz, an appreciable value is found up to z = 3 mm. After the radiation is switched off, the heating propagates mainly toward the internal tissues (the radial diffusion is significantly lower), and the peak value of the temperature elevation quickly decreases.

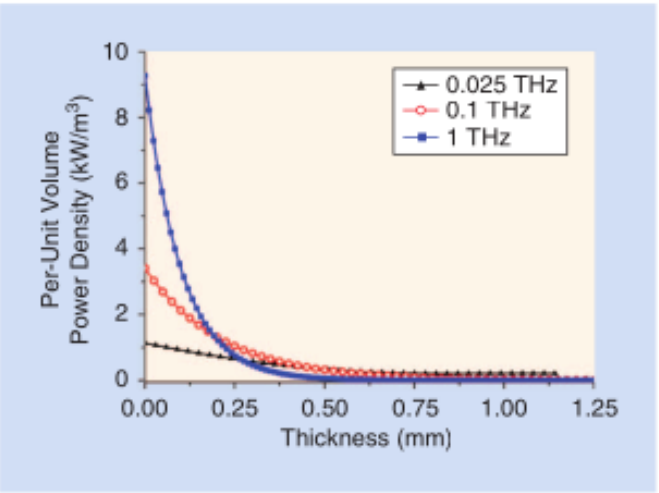

Figure 2. *A diagram along the z-axis of per-unit volume power density deposited by the wave in the tissues.*

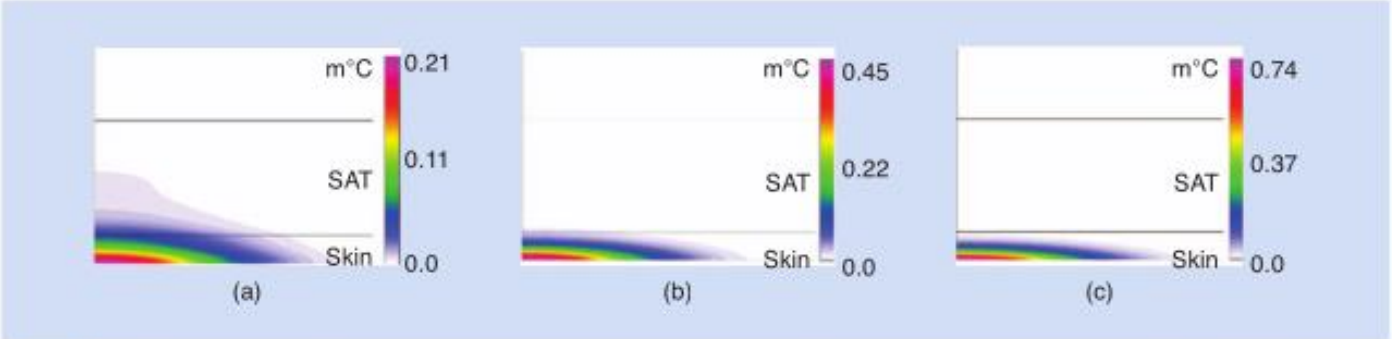

Figure 3. *Chromatic maps of the temperature elevation on an rz-plane (radius = 5 mm) at t = 1 s for (a) the 0.025-THz wave, (b) the 0.1-THz wave, and (c) the 1-THz wave.*

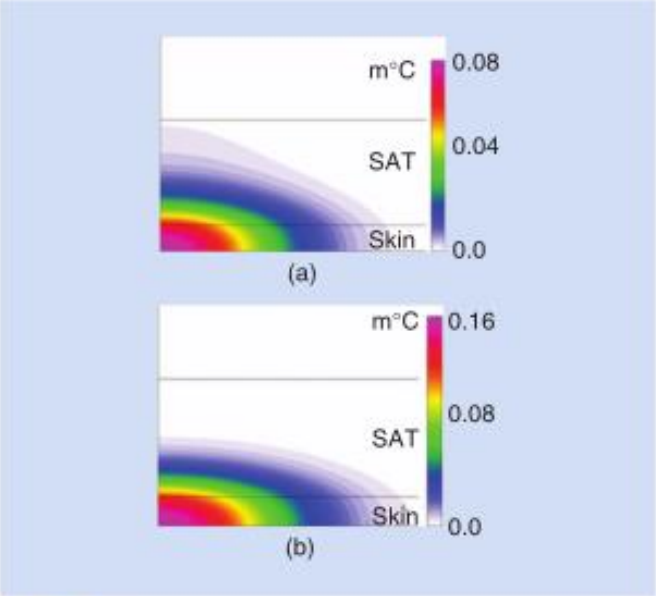

Figure 4. *Chromatic maps of the temperature elevation on an rz-plane (radius = 5 mm) at t = 8 s for (a) the 0.025-THz wave and (b) the 1-THz wave.*

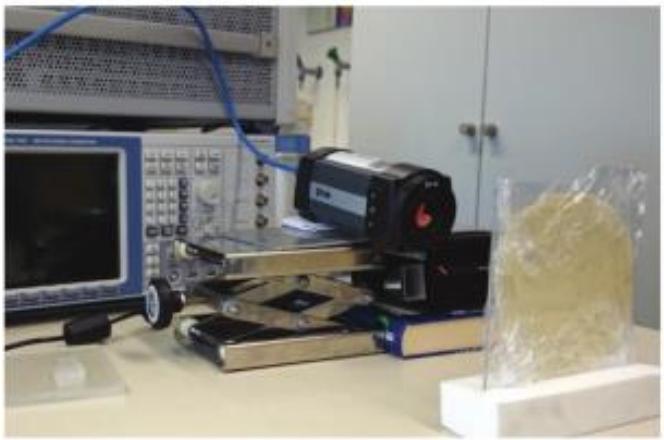

Figure 5. *The exposure setup, including the human skin phantom, an infrared camera, and a horn antenna as the radiation source.*

Measurement of Temperature Elevation Based on Thermal Imaging of Skin Phantoms

To verify the results from numerical simulations, a phantom having electrical and thermal properties comparable to human skin [13] has been exposed to microwave radiation and monitored with thermal infrared imaging. For the simple, practical setup shown in Figure 5, the skin phantom has been prepared with a gel layer (2-mm thick) composed of TX151 powder (25%) and water (75%) spread on a Plexiglass holder (3-mm thick). An RF generator (Agilent E8257D) at 35 GHz with an external power amplifier (Centellax TA2U50HA: typical gain 24–25 dB; typical output power up to 24–27 dBm) has been used to feed a horn antenna (Flann 23240-20, with coaxial-to-waveguide adaptor 23094-VF50) that serves as a radiation source at a distance of 10 cm from the human skin phantom. The sample is illuminated with a nearly Gaussian-shaped beam [14] having a beam waist of approximately 2.25 cm and a maximum radiation power density of approximately 40 mW/cm^2. The resulting temperature increase is measured with a conventional infrared camera (FLIR SC300) using background noise (on the order of 0.5 K) subtraction. Based on a large number of experiments using different samples, we estimate the expanded measurement uncertainty for the extraction of temperature differences to 0.2 K ($k = 2$, confidence interval 95%).

Comparison of Measurements and Simulations

Using the thermal and electrical properties either found in the literature or measured with a free-space spectrometer setup based on horn antennas and vector network analysis [4], simulations of the temperature elevation in the skin phantom were performed using an FEM [12]. Figure 6 shows the comparison of our simulations with measurements for different values of the heat transfer parameter h_{amb}, which describes the heat transfer between the phantom and the surrounding air.

The simulated temperature elevations are still subject to considerable uncertainty, which is due mainly to the uncertainty of the power radiated by the antenna, the parameters of the approximated Gaussian beam, and the uncertain thermal and electrical parameters of the gel phantom. However, measurements and simulations match well, within the expected measurement

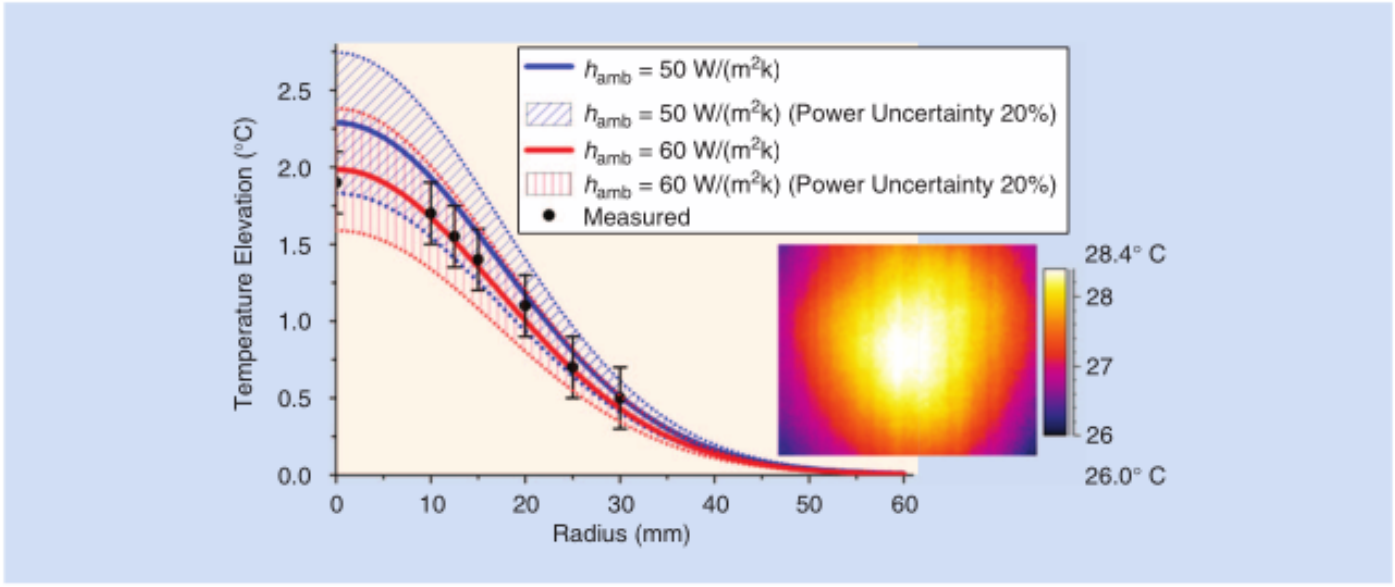

Figure 6. *The simulated temperature increase compared to the measured values extracted from the thermal image (shown in the inset) taken after 900 s of RF exposure.*

uncertainties. While the measurement uncertainty for temperature extraction is assumed to be 0.2 K (k = 2, confidence interval 95%), the uncertainty of the simulations (resulting from uncertainties in radiated power, sample alignment and accurate sample-to-antenna phase center distance, beam parameters, and thermal and electrical parameters) is estimated to be in the order of 20%.

Conclusions

We have demonstrated an approach for assessing the power densities radiated by security scanners and described in detail a methodology for simulating the resulting heat transfer to the human skin. We have also illustrated a simple and practical measurement setup based on the illumination of a gel phantom with millimeter-wave radiation and temperature measurements based on thermal imaging. The measurements show that the simulations are realistic and, therefore, can be used to predict the heat transfer to the human skin. Further work on simulations and measurements, e.g., related to the heating of the eyes, are intended.

Acknowledgments

We acknowledge funding as part of the European Metrology Research Program (EMRP) for the joint research project "Microwave and Terahertz Metrology for Homeland Security" (JRP NEW07–THz Security). The EMRP is jointly funded by the participating countries of the European Association of National Metrology Institutes (EURAMET e.V.) and the European Union.

References

[1] International Commission on Non-Ionizing Radiation Protection, "ICNIRP guidelines: For limiting exposure to time varying electric magnetic and electromagnetic fields (up to 300 GHz)," *Health Phys.*, vol. 74, pp. 494–522, 1998.

[2] EMRP Joint Research Project NEW07 THz Security, Security scanners–adequate methods to measure the exposure, best practice user guide. (Jan. 2015). [Online]. Available: http://www.ptb.de/emrp/804.html

[3] H. G. Unger, *Hochfrequenztechnik in Funk und Radar*. Stuttgart: Teubner, 1994.

[4] A. Kazemipour, M. Charles, D. Allal, M. Borsero, L. Zilberti, O. Bottauscio, M. Chiampi, T. Kleine-Ostmann, and T. Schrader, "Measurement and simulation of heat transfer into a human skin phantom," presented at the 40th International Conf. Infrared, Millimeter, and Terahertz Waves, Hong Kong, China, 2015.

[5] D. Andreuccetti, R. Fossi, and C. Petrucci, An internet resource for the calculation of the dielectric properties of body tissues. (Sept. 2015). [Online]. Available: http://niremf.ifac.cnr.it/tissprop/

[6] P.A. Hasgall, E. Neufeld, M.C. Gosselin, A. Klingenböck, and N. Kuster, (Feb. 2013). ITIS Database for thermal and electromagnetic parameters of biological tissues, Version 2.3. [Online]. Available: www.itis.ethz.ch/database.

[7] A. J. Fitzgerald, E. Berry, N. N. Zinov'ev, S. Homer-Vanniasinkam, R. E. Miles, J. M. Chamberlain, and M. A. Smith, "Catalogue of human tissue optical properties at terahertz frequencies," *J. Biol. Phys*, vol. 129, pp. 123–128, 2003.

[8] G. J. Wilmink, B. L. Ibey, T. Tongue, B. Schulkin, N. Laman, X. G. Peralta, C. C. Roth, C. Z. Cerna, B. D. Rivest, J. E. Grundt, and W. P. Roach, "Development of a compact terahertz time-domain spectrometer for the measurement of the optical properties of biological tissues," *J. Biomed. Opt.*, vol. 16, no. 4, 047006, Apr. 2011.

[9] E. Pickwell, B. E. Cole, A. J. Fitzgerald, V. P. Wallace, and M. Pepper, "Simulation of terahertz pulse propagation in biological systems," *Appl. Phys. Lett.*, vol. 84, no. 12, pp. 2190–2192, Mar. 2004.

[10] L. Zilberti, A. Arduino, O. Bottauscio, and M. Chiampi, "Parametric analysis of transient skin heating induced by terahertz radiation," *Bioelectromagnetics*, vol. 35, no. 5, pp. 314–323, July 2014.

[11] L. Zilberti, D. Voyer, O. Bottauscio, M. Chiampi, and R. Scorretti, "Effect of tissue parameters on skin heating due to millimeter EM waves," *IEEE Trans. Magn.*, vol. 51, no. 3, 9400904, Mar. 2015.

[12] O. Bottauscio, M. Chiampi, and L. Zilberti, "Thermal analysis of human tissues exposed to focused beam THz radiations," *IEEE Trans. Magn.*, vol. 51, no. 3, pp. 7400504, Mar. 2015.

[13] G. C. Walker et al. "Materials for phantoms for terahertz pulsed imaging," *Phys. Med. Biol.*, vol. 49, pp. N363, 2004.

[14] A. Kazemipour, M. Hudlicka, R. Dickhoff, M. Salhi, T. Kleine-Ostmann, and T. Schrader, "The horn antenna as gaussian source in the mm-wave domain—analytical study and measurement results," *J. Infrared Milli Terahz Waves*, vol. 35, pp. 720–731, 2014.